Scripta Materialia 204 (2021) 114125

Contents lists available at ScienceDirect

Scripta Materialia

journal homepage: www.elsevier.com/locate/scriptamat

Role of *in-situ* splat sintering on elastic and damping behavior of cold sprayed aluminum coatings

Tanaji Paul, Pranjal Nautiyal, Cheng Zhang, Benjamin Boesl, Arvind Agarwal*

Plasma Forming Laboratory, Florida International University, 10555 West Flagler Street, Miami, FL 33174, United States

ARTICLE INFO

Article history:
Received 6 June 2021
Revised 2 July 2021
Accepted 5 July 2021
Available online 13 July 2021

Keywords:
Damping
Elastic modulus
Dynamic mechanical analysis
Aluminum 6061
Heat treatment

ABSTRACT

The dynamic elastic behavior of cold sprayed aluminum 6061 coatings is analyzed to understand the inherent role of *in-situ* splat sintering from ambient to 400 °C for air and helium sprayed coatings. Higher surface energy and lower flattening ratio of air sprayed coating in as-sprayed condition result in 28% densification during splat sintering compared to 15% in heat-treated helium sprayed ones. Elastic modulus and damping behavior can be divided into three distinct temperature regimes based on sintering and progressive inter-splat structure. A theoretical analysis is established, which shows that normalized elastic modulus is an exponential function of the inter-splat porosity. This study establishes the correlation between inter-splat thermal phenomena and coating's dynamic mechanical properties at elevated temperatures.

Cold spray is a rapidly growing technology that has garnered significant interest in surface engineering [1] and additive manufacturing [2,3] research communities. In this process, metallic powder particles in the solid-state are accelerated at supersonic velocities on a substrate using a carrier gas. The manufactured coating exhibits a hierarchical structure from a dense deposit at the bulk to individual deformed particles or 'splats' at the microscopic level. These splats constitute the characteristic building blocks of cold sprayed coatings, with their mutual structural and mechanical interactions determining the macroscopic performance of the coatings [4,5]. One such parameter, elastic modulus, is a key characteristic and a manifestation of the inter-splat behavior. In the literature, the elastic modulus of cold sprayed coatings has been measured by tension [6], compression [7], high-load indentation [8], and 3-point fracture tests [9] at the macroscopic level to micropillar compression [10], and nanoindentation [11] at the microscopic one. While providing a preliminary look into the elastic behavior of cold sprayed coatings, these methods pose two significant challenges. First, the hierarchical splat structure introduces a delay or phase lag between the imposed stress and the resulting strain that cannot be captured by bulk quasi-static tests [12]. Second, localized nanoindentation tests, while providing insight into the interior of an individual splat, cannot enumerate the inter-splat elastic response [11]. It is important to investigate phase delay resulting from the unique hierarchical splat structure of the coating. Deformation of this hierarchical structure in applications with cyclic loading such as fatigue accumulates over time and is controlled by inter-splat phenomena [12]. This cyclic deformation can be investigated only by dynamic measurement techniques.

To address this gap in scientific knowledge, this study investigates the *in-situ* splat sintering phenomena in cold sprayed aluminum (Al 6061) coatings manufactured using air and helium carrier gases in as-sprayed and heat-treated conditions by dynamic mechanical analysis (DMA) technique. Material selection and processing were designed such that these particle surface phenomena are easily manifested and measurable. First, Al 6061 inter-particle surface phenomena such as sintering and oxidation initiate at relatively low temperatures [13,14]. Second, in-flight particle surface oxidation is influenced mainly by a cold spray carrier gas such as air, nitrogen, or helium [15]. Third, inter-splat surface bonding has been extensively reported to be controlled by post-spray heat treatment [16]. The analysis delves into the 'sweet spot' of dynamic and bulk response to simultaneously elucidate macroscopic elastic behavior and inter-splat damping energy losses. En route, this study constitutes the first report of *in-situ* splat sintering in the cold sprayed Al 6061 coatings and its effect on their elastic modulus. Finally, it establishes the scientific correlations between inter-splat thermal phenomena and coating mechanical properties.

Al 6061 powder was cold sprayed on Al 6061 substrate with air and helium as carrier gases using process conditions detailed in the authors' earlier publications [11,12]. To eliminate the effect of substrate and measure phenomena representative of the coatings alone, they were machined off from the substrate. In addition

* Corresponding author.
E-mail address: agarwala@fiu.edu (A. Agarwal).

https://doi.org/10.1016/j.scriptamat.2021.114125
1359-6462/

to as-sprayed ones, coatings were subjected to the commonly employed heat treatment at 176 °C for 1 h in an argon atmosphere [17]. Microstructures at the cross-sections of coatings, acquired using a scanning electron microscope (SEM) (JEOL, JSM 6330F), were utilized to calculate porosity using image analysis software, ImageJ. Elastic modulus, E (GPa) and damping, tan δ of the as-sprayed and heat-treated coatings were measured on specimens with dimensions 10 mm x 4 mm x 1 mm using a dynamic mechanical analyzer (NETZSCH, DMA 242 E Artemis). A 9.9 N static force, 9.0 N dynamic force, 30.0 μm amplitude, and a frequency of 5.0 Hz were employed. To maintain equilibrium, a slow *in-situ* heating rate of 3 °C min^{-1} was used to increase the temperature from ambient to 400 °C. It is emphasized here that the external (or *ex-situ*) heat treatment in the argon atmosphere occurs at a low temperature, 176 °C, for 1 h. In comparison, *in-situ* splat sintering occurs at a higher temperature range up to 400 °C for 2 h 13 min. 176 °C is lower than all temperatures at which sintering of aluminum has been reported. Since sintering exponentially increases with temperature [18], densifications at a lower temperature coupled with lower time are not investigated. Only *in-situ* splat sintering, one that occurs during continuous elastic modulus measurement, is analyzed.

The evolution of elastic modulus and damping of the air and helium sprayed Al 6061 coatings in as-sprayed and heat-treated conditions during heating is presented in Fig. 1. The hierarchical structure from a coating at the bulk to splats at the microscopic level can be correlated to its corresponding *in-situ* dynamic response. At the bulk level, the elastic modulus of all the coatings decreases with increasing temperature due to the higher stretching of atomic bonds by increased thermal vibrations [19]. Air sprayed coatings exhibit lower elastic modulus at the microscopic level than helium sprayed ones due to inferior metallurgical bonding and adhesion between splats resulting from higher in-flight oxide inclusions [20]. Heating introduces *in-situ* splat sintering and porosity mitigation, thereby increasing the elastic modulus of both coatings. Since helium spraying results in an already dense coating, there is a lower free energy incentive for splat sintering. Hence the extent of increase is lower than that of air sprayed coating. Damping, presented as tan δ, measures inter-splat energy loss in the coatings during dynamic deformation. With increased temperature, higher energy loss is observed in air sprayed coatings due to greater thermal vibrations of Al 6061 and oxide inclusions. In helium sprayed coatings, with significantly lesser oxide inclusions, this increase is much less pronounced. Additionally, in the air-sprayed coating, this loss is higher in as-sprayed conditions than heat-treated ones due to more significant inter-splat interfaces and porosity.

The phenomenon of *in-situ* splat sintering and porosity mitigation is illustrated by a schematic presented in Fig. 2. The air sprayed coating (Fig. 2a) is constituted of splats, represented in grey, with relatively more oxide inclusions on their surfaces, represented by black layers. The resulting inter-splat porosity is higher at ambient temperature. Under the action of the DMA probe, dynamic vibrations of oxide layers result in higher energy loss and reduced *in-situ* splat sintering, due to which the inter-splat porosity reduces only by a limited extent at elevated temperature (Fig. 2b). In contrast, the helium sprayed coating (Fig. 2c) consists of splats, represented in grey, that do not have oxide inclusions on their surfaces. The corresponding inter-splat porosity is also lower at ambient temperature. There is no energy loss from dynamic vibrations of oxides, and higher densification results in an almost entirely dense coating at elevated temperature (Fig. 2d).

Based on hierarchical phenomena occurring over progressively higher temperatures, the evolution of elastic modulus and damping can be divided into 3 distinct regimes (Fig. 1). There is no significant sintering between adjacent splats in Regime 1 at low temperatures from ambient to 200 °C. The elastic modulus thus continues to decrease with increasing temperature due to increasing atomic vibrations [19]. In Regime 2 at 200 – 275 °C, *in-situ* splat sintering and pore mitigation occurred. Here, two factors are operational, namely (1) pore mitigation and (2) atomic vibrations. With increasing temperature, T, pore mitigation increases elastic modulus, E and hence the slope of E vs T should be positive. On the other hand, with increasing temperature, atomic vibrations reduces elastic modulus and thus slope of E vs T should be negative [19]. There is opposing competition between the positive and negative slopes. Thus, in this regime, the rate of reduction of elastic modulus with temperature or slope of E vs T plots is reduced (Fig. 1a). A similar decrease of the slope is observed in the damping plots, albeit to a lesser extent. Finally, in Regime 3 from 275 – 400 °C, the elastic modulus of the *in-situ* sintered coatings continues to decrease at a slower rate with increasing temperature. At 400 °C, the elastic modulus of wrought Al 6061 has been reported to be 53 - 56 GPa, i.e., 75 – 80% of that at ambient temperature [21]. In the air and helium sprayed coatings, the elastic modulus at 400 °C is measured to be 17 – 22 GPa and 38 - 39 GPa, i.e., 24 – 32% and 54 - 55%, respectively to that of wrought Al 6061 at ambient temperature. It can be concluded that at the same temperature, the elastic moduli of both coatings with a microscopic splat structure are lower than that of a wrought alloy structure. Simi-

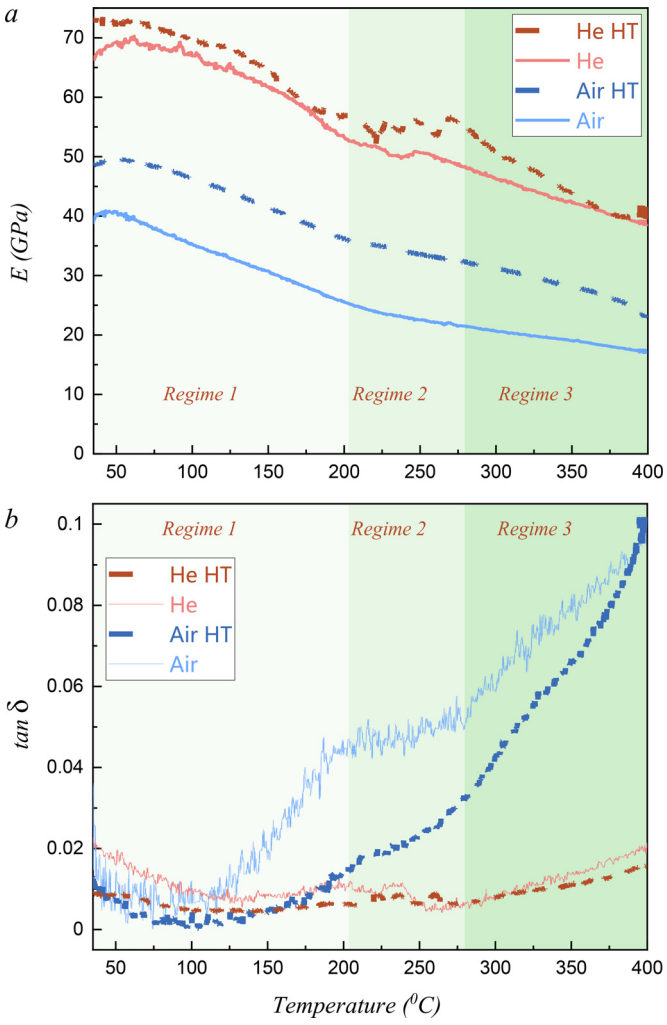

Fig. 1. Three regimes in the evolution of (a) elastic modulus and (b) damping with temperature in air (Air) and helium (He) cold sprayed Al 6061 coatings in as-sprayed and heat-treated (HT) conditions.

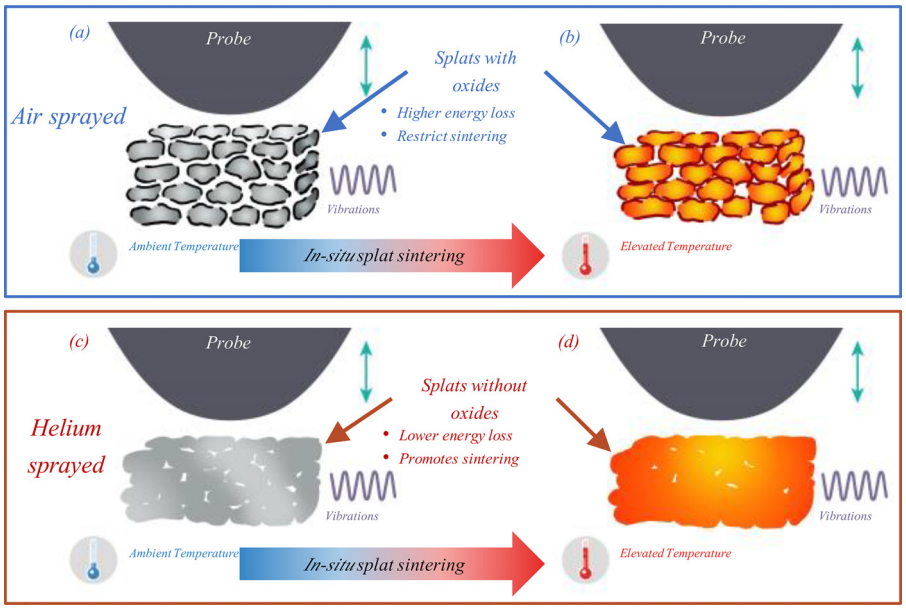

Fig. 2. Schematic illustrating the phenomenon of *in-situ* splat sintering in air and helium cold sprayed Al 6061 coatings.

lar to elastic modulus, the damping, tan δ in Regime 2 confirms *in-situ* splat sintering phenomenon. Without sintering, the value of damping would have increased continuously with increasing temperature [22–24]. Due to sintering in Regime 2, there is an arrest in this increase. Particularly for air sprayed coating in as-sprayed condition, where the sintering is maximum, the graph becomes almost flat. The manifestation of these changes in slopes, simultaneously in elastic modulus and damping confirms the phenomenon of *in-situ* splat sintering which is quantified in the following sections.

In-situ splat sintering is quantified and correlated with mechanical response in two steps. First, at ambient temperature, the inter-splat porosity is calculated using only the measured normalized elastic modulus of the coatings. Second, at 400 °C the volume fraction of inter-splat porosity is computed using the normalized elastic modulus and assuming a linear modulus-temperature relationship in the absence of sintering. Comparing the actual measured value with the one assuming an absence of sintering enables the evaluation of densification during splat sintering. The normalized elastic modulus is defined as E_c/E_b where E_c and E_b (GPa) are the elastic moduli of the coating and wrought Al 6061, respectively. In cold sprayed coatings, inter-splat pores are oriented parallel to the coating plane and are treated horizontally aligned pores [25,26]. Under this condition, according to the analytical Zimmerman model [27], the normalized elastic modulus reduces to

$$\frac{E_c}{E_b} = \frac{1}{1+5C} \tag{1}$$

Where C represents the volume density of inter-splat pores. From the measured elastic modulus, the inter-splat pore density is calculated and presented in Fig. 3a. The porosity of air sprayed coatings is significantly higher than helium sprayed ones from restriction to bonding from in-flight surface oxide inclusions. In addition, the density improves due to enhancement in bonding upon heat treatment in both the coatings with the helium sprayed heat-treated coating exhibiting a near fully dense structure. This trend agrees with the two-dimensional porosity observed in the cross-sectional SEM micrographs of the coatings, presented in Fig. 3b.

This first step also enables the unification of the normalized elastic modulus of Al 6061 cold sprayed coatings, independent of carrier gas and heat treatment, under the aegis of a single analytical relationship utilizing their flattening ratio and fraction of porous boundaries. The flattening ratio for the air and helium sprayed Al 6061 coatings sprayed by the authors and investigated in this study are $\alpha_{air} = 1.04$, and $\alpha_{helium} = 1.60$ [12]. The number of splat boundaries per unit volume of the coating, N_v (m^{-3}) is [27,28],

$$N_v = \frac{1}{\pi R^3 \alpha^2 \beta} \tag{2}$$

Where R (m) is the radius of the powder particles, and β is the ratio of splat thickness to powder particle radius. Since the volume of powder particles is conserved during splat formation, α and β are related as

$$\alpha^2 \beta = \frac{4}{3} \tag{3}$$

The fraction of porous boundaries, f equals

$$f = \frac{4\pi C}{3\alpha^3} \tag{4}$$

Since α_{air} and α_{helium} are known, the normalized elastic modulus of cold sprayed Al 6061 coatings can be correlated to their fraction of porous boundaries as

$$\frac{E_c}{E_b} = 0.9(1+f)^{-1.2} \tag{5}$$

In the second step, the extent of densification during *in-situ* splat sintering is quantified. The procedure is explained using measurements for air sprayed coating in as-sprayed condition as representative. In the absence of a hierarchical structure without individual splats, no sintering would occur. The elastic modulus of cold sprayed coating would continue to decrease linearly with temperature [21], shown by the broken extrapolated line in Fig. 4a. In the presence of *in-situ* splat sintering, the actual measured elastic modulus is higher than the solid line. An identical procedure is followed for all the coatings and the values are used to calculate the sintering densification of all four coatings shown in Fig. 4b.

It is observed that as-sprayed coatings exhibit higher densification than heat-treated ones. This is because as-sprayed coatings have inter-splat pores that increase the total surface energy of the coatings. Hence there is a higher driving force for densification to occur. Upon heat treatment, metallurgical bonding and adhesion between the splats are enhanced, reducing the surface energy and

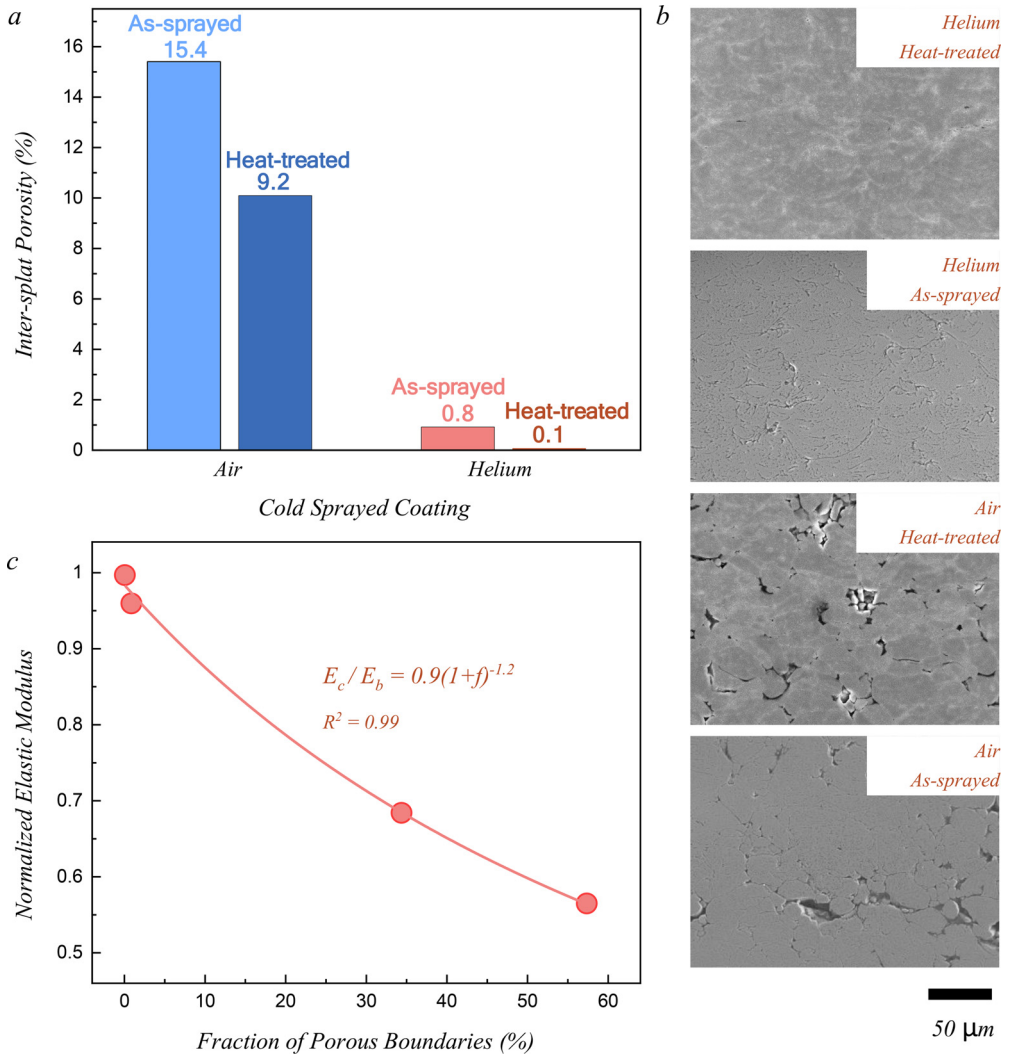

Fig. 3. (a) Inter-splat pore density in air and helium sprayed cold sprayed Al 6061 coatings in as-sprayed and heat-treated conditions. (b) Two-dimensional porosity was observed in the cross-sectional SEM micrographs of the coatings. (c) Unified correlation of the normalized elastic modulus of cold sprayed Al 6061 coatings to their structure independent of carrier gas and heat treatment.

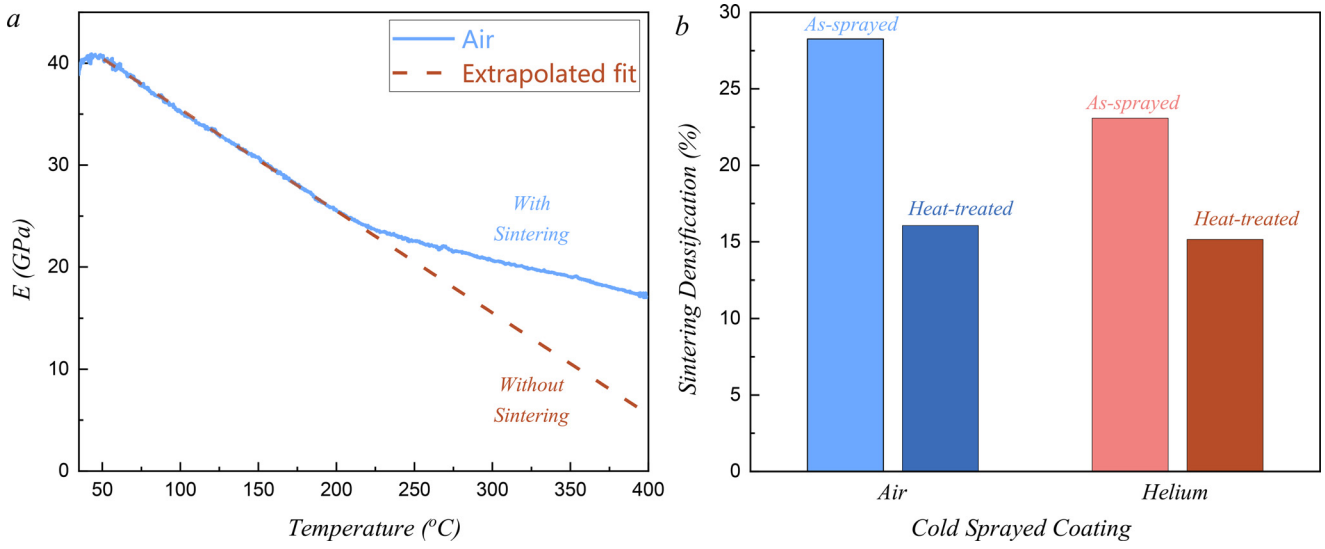

Fig. 4. (a) Increase in measured elastic modulus due to *in-situ* splat sintering compared to that in the absence of sintering. Shown for air sprayed Al 6061 coating in as-sprayed condition as representative. Identical procedure is followed for all coatings to calculate (b) densification during *in-situ* splat sintering in air and helium cold sprayed Al 6061 coatings in as-sprayed and heat-treated conditions.

driving force for densification. Air sprayed coatings exhibit higher densification since their flattening ratio, 1.04, is lower, providing the splats higher space for rearrangement and filling inter-splat pores. Helium sprayed splats with a higher flattening ratio, 1.60, have lesser space to rearrange and fill pores. However, the role of the flattening ratio on densification becomes less dominant in heat-treated coatings, manifested by the negligible difference in densifications.

The key conclusions derived from this study are summarized below.

1 Inter-splat structure and thermal phenomena are the chief controlling factors that determine the dynamic elastic response such as modulus, phase lag, and damping energy loss in cold sprayed aluminum coatings.
2 The normalized elastic modulus decreases exponentially with the fraction of porous boundaries that reduce with helium spraying and heat treatment.
3 *In-situ* splat sintering, occurring during heating, enhances the elastic modulus of the coatings compared to that without a hierarchical structure.
4 The surface energy of the splat structure and flattening ratio of the Al 6061 coatings investigated in this study determine the extent of *in-situ* splat sintering densification, with the latter's effect being less dominant in heat-treated coatings.

These conclusions provide the design and operating windows for cold sprayed structural and aerospace components exposed to harsh, high-temperature environments.

Declaration of Competing Interest

The authors declare that they have no known competing financial interests or personal relationships that could have appeared to influence the work reported in this paper.

Acknowledgment

The authors gratefully acknowledge support from the Army Research Laboratory through the W911NF2020256 grant. Usage of facilities at the Advanced Materials Engineering Research Institute (AMERI) is recognized for the research reported in this study. The authors acknowledge the assistance of Ms. Maria Mendez in the preparation of the schematic illustrations.

Supplementary materials

Supplementary material associated with this article can be found, in the online version, at doi:10.1016/j.scriptamat.2021.114125.

References

[1] S.M. Hassani-Gangaraj, A. Moridi, M. Guagliano, Surf. Eng. 31 (2015) 803–815.
[2] S. Pathak, G.C. Saha, Coatings 7 (8) (2017) 1–27.
[3] W. Li, K. Yang, S. Yin, X. Yang, Y. Xu, R. Lupoi, J. Mater. Sci. Technol. 34 (2018) 440–457.
[4] C.M. Sample, V.K. Champagne, A.T. Nardi, D.A. Lados, Addit. Manuf. 36 (2020) 1–17.
[5] A. Moridi, S.M. Hassani-Gangaraj, M. Guagliano, M. Dao, Surf. Eng. 30 (2014) 369–395.
[6] N. Kang, P. Coddet, H. Liao, C. Coddet, Surf. Coat. Technol. 280 (2015) 64–71.
[7] M.S. Baek, H.J. Kim, K.A. Lee, J. Nanosci. Nanotechnol. 19 (2019) 3935–3942.
[8] M. Winnicki, L. Łatka, M. Jasiorski, A. Baszczuk, Surf. Coat. Technol. 405 (2021) 1–11.
[9] S.R. Bakshi, T. Laha, K. Balani, A. Agarwal, J. Karthikeyan, Surf. Eng. 23 (2007) 18–22.
[10] A. Kurdi, T. Tabbakh, H. Alhazmi, Surf. Coat. Technol. 403 (2020) 1–8.
[11] P. Nautiyal, C. Zhang, V. Champagne, B. Boesl, A. Agarwal, Surf. Coat. Technol. 372 (2019) 353–360.
[12] P. Nautiyal, C. Zhang, V.K. Champagne, B. Boesl, A. Agarwal, Mater. Sci. Eng. A 737 (2018) 297–309.
[13] L.P.H. Jeurgens, W.G. Sloof, F.D. Tichelaar, E.J. Mittemeijer, J. Appl. Phys. 418 (2002) 89–101.
[14] H. Kwon, D.H. Park, Y. Park, J.F. Silvain, A. Kawasaki, Y. Park, Met. Mater. Int. 16 (2010) 71–75.
[15] H. Assadi, H. Kreye, F. Gärtner, T. Klassen, Acta Mater. 116 (2016) 382–407.
[16] W.Y. Li, C.J. Li, H. Liao, J. Therm. Spray Technol. 15 (2006) 206–211.
[17] M.R. Rokni, C.A. Widener, O.C. Ozdemir, G.A. Crawford, Surf. Coat. Technol. 309 (2017) 641–650.
[18] T.T. Fang, J.T. Shiue, F.S. Shiau, Mater. Chem. Phys. 80 (2003) 108–113.
[19] L. Yu, Y. Ma, C. Zhou, H. Xu, Int. J. Solids Struct. 42 (2005) 3045–3058.
[20] K. Kim, S. Kuroda, M. Watanabe, R. Huang, H. Fukanuma, H. Katanoda, J. Therm. Spray Technol. 21 (2012) 550–560.
[21] M.N. Su, B. Young, Thin Walled Struct 140 (2019) 506–515.
[22] D. Siva Prasad, P.T. Radha, C. Shoba, P.S. Rao, J. Alloys Compd. 767 (2018) 988–993.
[23] D.S. Prasad, C. Shoba, K.R. Varma, A. Khurshid, J. Alloys Compd. 646 (2015) 257–263.
[24] B. Pricop, E. Mihalache, M.N. Lohan, B. Istrate, M. Mocanu, B. Ozkal, L.G. Bujoreanu, in: MATEC Web Conferences, 33, EDP Sciences, 2015, pp. 1–6.
[25] V. Luzin, K. Spencer, M.X. Zhang, Acta Mater. 59 (2011) 1259–1270.
[26] N.M. Chavan, M. Ramakrishna, P.S. Phani, D.S. Rao, G. Sundararajan, Surf. Coat. Technol. 205 (2011) 4798–4807.
[27] R.W. Zimmerman, J. Mater. Sci. Lett. 4 (1985) 1457–1460.
[28] N. Laws, J.R. Brockenbrough, Int. J. Solids Struct. 35 (1987) 721–742.